УДК 528.9:556.162:004.94 DOI: https://doi.org/10.24028/gj.v48i2.346831

Validation of global elevation models using ICESat-2 LiDAR data for floodplain modeling in the Ukrainian Carpathians

V.V. Nikoriak, V.V. Osypov, N.M. Osadcha, 2026

Ukrainian Hydrometeorological Institute, Kyiv, Ukraine
Received 16 December 2025

Accurate topographic data underpin hydrological and floodplain modeling in mountainous environments where steep gradients and dense forest cover amplify vertical errors in global Digital Elevation Models (DEMs). This study performs a comprehensive validation of freely available DEMs — SRTM v3, NASADEM, ASTER GDEM v2, ALOS AW3D30, Copernicus GLO-30, FABDEM, and TanDEM-X — against high-precision Ice, Cloud, and land Elevation Satellite-2 (ICESat-2) LiDAR altimetry within the Ukrainian Carpathians. To ensure geodetic consistency, all DEMs and ICESat-2 observations were vertically transformed to the European Vertical Reference System (EVRS) using the high-resolution European Gravimetric Quasi-Geoid EGG2015 prior to analysis.

Elevation residuals were quantified using both classical (Mean Error, Root Mean Square Error) and robust (Normalized Median Absolute Deviation) statistical metrics, combined with terrain-stratified analysis based on slope, land cover, and hydrological position derived from the Height Above Nearest Drainage (HAND) model. The results demonstrate that DEM errors are strongly controlled by terrain steepness and vegetation cover, with non-linear error amplification observed in slopes exceeding 12° and in forested areas.

Among the tested datasets, FABDEM demonstrates the lowest mean error (≈1.5 m) and the highest stability across all slope classes. In contrast SRTM and NASADEM systematically overestimate elevations in forested terrain due to canopy effects. Copernicus GLO-30 and ALOS AW3D30 exhibit moderate accuracy but degraded performance beyond 15° slopes. ASTER GDEM displayed the largest variability and extreme errors, particularly in complex terrain.

Hydrological analysis revealed that DEM-related uncertainties propagate directly into floodplain modeling outputs. Within the critical HAND 0—6 m zone, vertical errors (5—10 m) were comparable to or exceeded typical flood depths, resulting in substantial discrepancies in inundation extent, channel geometry, and hydraulic parameters.

The study further demonstrates that compliance with international accuracy standards (INSPIRE, FEMA, LAWA) is generally limited to low-relief terrain, whereas most global DEMs fail to meet requirements in mountainous regions. These findings highlight the necessity of using DTM-type datasets or LiDAR-derived elevation models for regulatory flood-risk assessments.

To support reproducible and scalable analysis, the study introduces the GeoHydroAI framework — an integrated geospatial analytical environment combining ICESat-2 processing via SlideRule, DEM differencing using xDEM, terrain analysis with WhiteboxTools, and high-performance spatial querying with DuckDB.

This approach enables automated validation, terrain-stratified error analysis, and interactive exploration of DEM uncertainty across geomorphological and hydrological gradients. The proposed framework establishes a reproducible standard for DEM evaluation and provides a data-driven foundation for flood-risk assessment and hydrological modeling in

Citation: Nikoriak, V.V., Osypov, V.V., & Osadcha, N.M. (2026). Validation of global elevation models using ICESat-2 LiDAR data for floodplain modeling in the Ukrainian Carpathians. *Geofizychnyi Zhurnal*, *48*(2), 35—59. https://doi.org/10.24028/gj.v48i2.346831.

data-scarce mountainous regions. Furthermore, the integration of geodetic referencing (EVRS/EGG2015), satellite altimetry (ICESat-2), and geomorphological analysis establishes a physically consistent framework for terrain representation in hydrological applications. This work positions DEM validation as a core component of GeoAI-driven environmental modeling, bridging geodesy, remote sensing, and hydraulic simulation within a unified analytical paradigm.

Key words: Digital Elevation Model, SRTM, Copernicus GLO-30, NASADEM, ALOS AW3D30, FABDEM, Height Above Nearest Drainage, floodplain modeling, hydrological accuracy, GeoHydroAI, Ukrainian Carpathians.

Introduction. Digital Elevation Models (DEMs) form a core geospatial layer in Geographic Information Systems, supporting terrain analysis, watershed characterization, erosion studies, and flood-risk mapping [Zhou, 2017]. A DEM represents the bare-earth surface, excluding vegetation and built structures, and differs from Digital Surface and Terrain Models [Li et al., 2005]. Numerous terrain attributes — slope, aspect, flow direction, stream order, and the Topographic Wetness Index — can be derived from DEMs to support the simulation of surface-water movement and landscape processes [Wilson, Gallant, 2000]. These derivatives enable flood modeling, soil moisture estimation, and groundwater recharge mapping, integrating DEM-based topography with remote-sensing and Geographic Information Systems layers [Zhou, Li, 2020].

DEM resolution and accuracy strongly influence hydrological modeling because terrain derivatives govern watershed delineation, flow routing, and Hydrological Response Unit definition. Errors or coarse interpolation degrade model realism, especially in flat or forested terrain [Wechsler, 2003; Moges et al., 2023; Alganci et al., 2018]. Xu et al. [2021] showed that discrepancies among open-access DEMs cause major variations in simulated floods, particularly in low-relief urban areas where vertical bias dominates. DEM generalization methods are equally critical: Chen et al. [2012] found that simplistic stream-burning distorts slopes and drainage, while compound Triangulated Irregular Network approaches preserve morphology and hydrological connectivity across scales. Zhu and Chen [2024] further demonstrated that coarsening DEMs from 30 m to 300—500 m reduces flood simulation accuracy by up to 38 %, mainly through stream network loss and slope flattening. Hence, hydrological realism requires a balance between computational efficiency and high-resolution, terrain-preserving generalization (≤30 m).

The Height Above Nearest Drainage (HAND) model estimates flood inundation by measuring each cell's elevation above the drainage network [Nobre et al., 2011]. Combined with synthetic rating curves and discharge estimates, HAND enables scalable inundation mapping but remains highly sensitive to DEM precision. High-resolution DEMs (1—2 m) yield agreement within 6—10 % of the reference maps, whereas coarse DEMs introduce significant spatial uncertainty [Hu, Demir, 2021]. Despite computational efficiency, HAND performance deteriorates in steep or infrastructure-rich areas where hydraulics are unresolved [Godbout et al., 2019].

Beyond geometry, DEMs discretize the gravitational potential field controlling surface flow. Slope represents the potential gradient that defines the energy available for runoff. Zhou et al. [2018] showed that vertical DEM errors distort estimates of gravitational force and discharge predictions, underscoring the need for a hydrologically consistent terrain representation. In hydraulic models such as HEC-RAS, preprocessing — depression filling, stream conditioning — is essential to restore realistic potential-energy gradients [Munir et al., 2020]. Coarse DEMs (90 m vs 30 m) typically overestimate inundation and underestimate depth, compromising hydrodynamic realism [Xu et al., 2021]. Similarly, Kenward et al. [2000] demonstrated that vertical inaccuracies delay and attenuate simulated peak flows. Overall, DEM quality — both

vertical accuracy and structural integrity — is fundamental to reliable runoff and flood modeling.

Despite their widespread use, publicly available global DEMs — such as Shuttle Radar Topography Mission (SRTM), Advanced Land Observing Satellite (ALOS AW3D30)[JAXA, 2021], Copernicus DEM Global (Copernicus GLO-30) [Airbus …, 2022], Forests And Buildings removed DEM (FABDEM) [Neal et al., 2023], TerraSAR-X/TanDEM-X mission (TanDEM-X), NASA Digital Elevation Model (SRTM reprocessed) (NASADEM), and Advanced Spaceborne Thermal Emission and Reflection Radiometer (ASTER GDEM) — often contain systematic and spatially variable errors. Historically, these datasets have been derived from radar interferometry (SRTM, TanDEM-X), optical stereo imagery (ALOS, ASTER), or hybrid processing with bias correction (FABDEM, Copernicus, NASADEM). Each generation has introduced refinements — improved vertical calibration, vegetation filtering, or gap filling — but their relative performance in mountainous terrain remains uncertain. Such uncertainty becomes critical in regions like the Ukrainian Carpathians, where steep slopes, dense canopy, and data scarcity amplify vertical deviations and degrade hydrological model accuracy.

Numerous studies have reported that DEM resolution and accuracy directly affect flood simulation outcomes [Garousi-Nejad et al., 2019; Mokhtar et al., 2018; Arash, Yasi, 2022; Aristizabal et al., 2024]. In the Bășeu River (Romania), [Stoleriu et al., 2020] showed that SRTM-based flood models underestimated inundated areas compared with Light Detection and Ranging (LiDAR) DEM results, missing critical zones in densely populated floodplains. Similarly, Farooq et al. [2019] found that ASTER GDEM overestimated flood depths by up to 18 m relative to observed data, whereas TanDEM-X (12 m) provided more realistic results. These findings emphasize that both vertical and planimetric accuracy are essential for reliable hydraulic simulations, particularly in steep or forested catchments.

The Ice, Cloud, and land Elevation Satellite-2 (ICESat-2) mission provides spaceborne photon-counting LiDAR measurements of surface elevation [Markus et al., 2017]. The ATL03 (geolocated photon heights) and ATL08 (classified terrain heights) data products provide high-precision elevation measurements that can be used as independent checkpoints for DEM validation. As a spaceborne photon-counting system, ICESat-2 provides independent, high-accuracy ground elevations (<1 m error), enabling statistical validation of DEMs even in areas without ground-based benchmarks. Although ICESat-2 offers sparse coverage (~0.7 m along-track spacing), its precision supports robust DEM error assessment using thousands of control points. Guenther et al. [2024] further demonstrated that ICESat-2 returns can train convolutional neural networks to correct TanDEM-X errors, reducing RMSE from 11.3 m to 4.4 m in forested terrain — highlighting its potential for large-scale DEM calibration.

However, few studies have assessed global DEMs using consistent vertical references. While Gdulová et al. [2020] analyzed TanDEM-X accuracy over Czech mountains, no comprehensive evaluation has yet covered all major open-access DEMs across the Ukrainian Carpathians. Previous Ukrainian works [Postelniak, 2013; Kovalchuk et al., 2019] compared SRTM, ASTER, and ALOS within the WGS-84/EGM96 system but did not convert their elevation values to the national vertical reference European Gravimetric Quasi-Geoid (EGG 2015), leaving geoid-related biases uncorrected. As geoid anomalies in the Carpathians reach 0.1—0.2 m [Zablotskyi et al., 2021], ignoring these offsets may compromise hydrological realism. Moreover, the impact of seasonal canopy phases (leaf-on vs. leaf-off) on DEM accuracy remains largely unexplored in this region.

Aim and novelty. This study presents a comprehensive evaluation of seven globally available DEMs — SRTM, ALOS AW3D30, Copernicus GLO-30, FABDEM, TanDEM-X, NASADEM, and ASTER GDEM — over the Bilyi Cheremosh River basin in the Ukrainian Carpathians. To ensure consistent reference, all DEMs were vertically transformed to the

EGG2015 and then validated against ICESat-2 ATL03/ATL08 ground returns. The analysis proceeds as follows: (1) pointwise accuracy metrics — Mean Error (ME), Mean Absolute Error (MAE), Root Mean Square Error (RMSE), and Normalized Median Absolute Deviation (NMAD); (2) terrain-dependent error propagation by slope, land cover, and hydrological position; (3) assessment of DEM suitability for hydrological and hydraulic modeling; and (4) development of the GeoHydroAI platform for automated processing, comparison, and visualization of multi-source DEM data, which enables reproducible analyses and modular integration of hydrological and hydraulic modeling tools.

Further, by interpreting DEMs as discretized representations of the gravitational-potential field rather than mere height grids, this research introduces a novel physical perspective on DEM quality assessment. To our knowledge, it is the first systematic comparison of all major open-access DEMs across the Ukrainian Carpathians using unified vertical referencing and ICESat-2 validation. These results contribute to improving regional flood modeling accuracy and advancing open, reproducible geospatial standards for mountainous terrains.

Data and Methods. ***Study area.*** This study focuses on the Bilyi Cheremosh River Basin, located in the Ukrainian Carpathians (Fig. 1).

The basin lies within the Chernivtsi and Ivano-Frankivsk Oblasts in western Ukraine and covers approximately 632 km^2.

Elevations range from 400 m to 1,900 m a.s.l., with steep mountain slopes typical of the Flysch Carpathians.

The Bilyi Cheremosh River (51 km in length) is characterized by a flash-flood regime driven by both rainfall and snowmelt, making it a representative watershed for evaluating DEMs in complex mountainous terrain.

The region is predominantly forested, with a mixed coniferous—deciduous canopy, which affects DEM accuracy due to canopy interference.

Standards for elevation models. Flood inundation modeling is highly sensitive to the vertical accuracy and spatial resolution of DEMs. Both the United States and the European Union have established institutional standards and guidelines to ensure the reliability of elevation data used in hydraulic and flood-risk modeling (Table 1 summarizes the

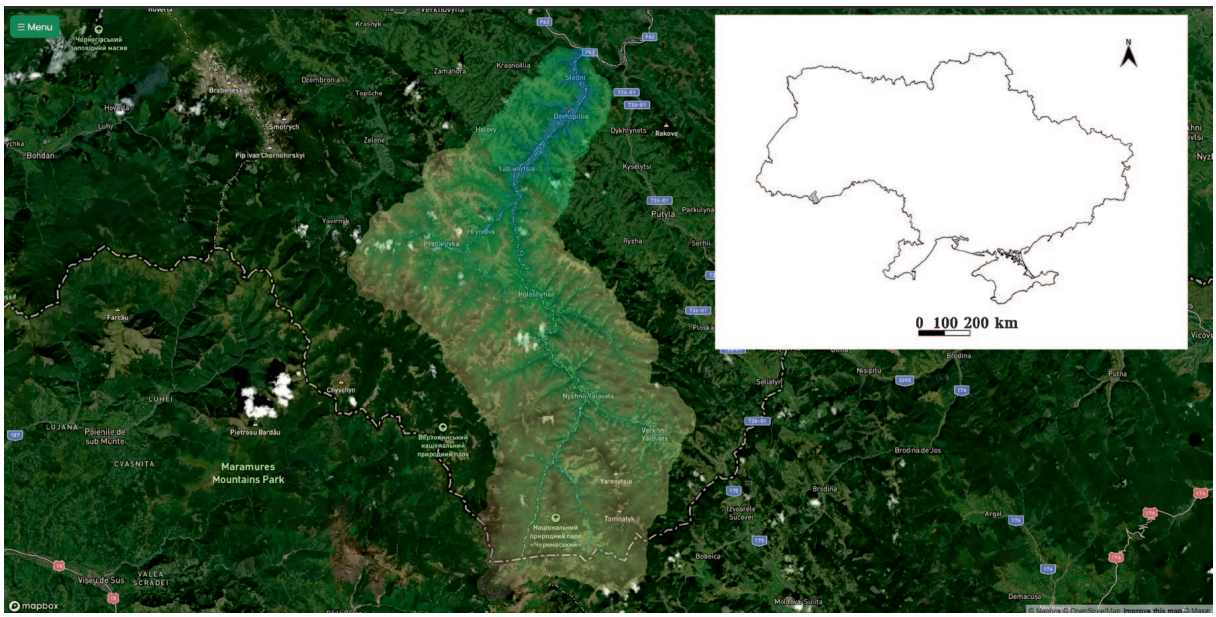

Fig. 1. Location of the Bilyi Cheremosh River Basin within the Ukrainian Carpathians. Screenshot extracted from the GeoHydroAI web-based analytical platform. Base map and satellite imagery © Mapbox, 2025. Projection: WGS84 (EPSG:4326).

main DEM accuracy standards applied in the USA, EU, and Ukraine).

In the United States, the Federal Emergency Management Agency (FEMA) formalized vertical accuracy standards through Standard ID 43 (SID 43), detailed in Guidance Document 27 [FEMA, 2016]. DEMs used for delineating Special Flood Hazard Areas must meet accuracy thresholds defined by terrain type and flood risk level. For example, flat, high-risk areas require a Fundamental Vertical Accuracy (FVA) of ≤24.5 cm and a Consolidated Vertical Accuracy (CVA) of ≤36.3 cm, with a LiDAR Nominal Pulse Spacing of ≤2 m. SID 43 thus serves as a regulatory benchmark for DEM evaluation in FEMA's hydraulic modeling practice.

Within the European Union, the Floods Directive [European … 2007] mandates Member States to produce flood hazard and risk maps but leaves the technical implementation to national authorities. The INSPIRE Directive and its Technical Guidelines for the Elevation Theme [European …, 2014] specify that elevation data must be referenced to ETRS89 (horizontal) and EVRS (vertical), typically realized as EVRF2000/2007 or the gravimetric geoid model EGG2015.

To maintain internal consistency between spatial resolution (GSD) and vertical accuracy, INSPIRE recommends that the vertical Root Mean Square Error (RMSEv) should not exceed one-third of the raster grid spacing (GSD/3). For example, a 30 m DEM should have RMSEv≤10 m, and a 10 m DEM should have RMSEv≤3.3 m. These criteria align with international standards such as ISO 19157 and CEN/TR 15449, which relate positional and vertical accuracy to data resolution.

INSPIRE Annex II-III further defines requirements for topological and thematic consistency of elevation vector datasets (contours, breaklines). In mountainous terrain, where vertical errors propagate nonlinearly into hydrodynamic simulations, national best practices often exceed these minimum requirements.

For instance, Germany's LAWA [LAWA, 2010] recommends Digital Terrain Models (DTMs) with a 2 m resolution and a vertical RMSE of 10—20 cm, typically derived from airborne LiDAR. In France, the IGN RGE ALTI® and Litto3D programs have transitioned to 1 m LiDAR-based DTMs with RMSE below 0.5 m [IGN, 2021].

In Ukraine, the Methodology for Flood

Table 1. Comparative overview of DEM standards and national practices for flood hazard and hydraulic modeling

Region/Program	Standard/Document	GSD[1]	Vertical Accuracy	Vertical Datum	Notes
USA (FEMA[2])	SID 43/Guidance Document 27 (2016)	≤2 m	FVA[3]≤24.5 cm CVA[3]≤36.3 cm	NAVD88	Required for SFHA zones; depends on risk level and terrain
EU (INSPIRE Directive)	Dir. 2007/60/EC; TWG Elevation Guidelines (2014)	10—30 m	RMSEv[5]≤GSD/3	ETRS89/ EVRS	Harmonized horizontal/ vertical reference for EU datasets
Germany (LAWA[6])	LAWA Recommendations (2010)	2 m	RMSEv[5] 1 0—20 cm	EVRS	LiDAR-based DTM for official flood mapping
France (IGN — RGE ALTI[7])	RGE ALTI® v2.0 Specification	1 m/5 m	LiDAR 0.2—0.5 m Radar ~7 m	IGN69/ RGF93/ LAMB93	National DTM with quality metadata
Ukraine	MIA Methodology No. 153 (2018)	—	High-resolution DTM+field surveys	EVRS	Mandatory for official 1D/2D flood models; EVRS alignment required

Notes: [1]GSD — Ground Sampling Distance; [2]FEMA — Federal Emergency Management Agency; [3]FVA/CVA — Fundamental/Consolidated Vertical Accuracy; [4]INSPIRE — Infrastructure for Spatial Information in the European Community; [5]RMSEv — Root Mean Square Error (vertical); [6]LAWA — German Working Group on Water Issues; [7]RGE ALTI® — «Référentiel à Grande Échelle — Altimétrie», France'snational DTM product.

Hazard and Risk Mapping [Order № 153, Ministry of Internal Affairs, 2018] was developed in line with the EU Floods Directive. It prescribes the use of high-resolution DTMs and ground survey data, 1:10,000 mapping scale, 1D/2D hydraulic models, and mandatory compliance with EVRS-based vertical referencing and geospatial metadata standards.

These international and national standards collectively emphasize the necessity of accurate, vertically consistent DEMs for hydrological and hydraulic modeling, ensuring comparability and interoperability across regions.

Satellite altimetry data. High-precision altimetric checkpoints were obtained from the ICESat-2 ATL03 (geolocated photon heights) and ATL08 (classified terrain heights) products for the period 2018—2024, with data acquisition and processing facilitated by the SlideRule Earth cloud platform [Swinski et al., 2025].

The ATL03 product provides individual photon events, while ATL08 classifies them into ground, canopy, and noise photons [Neuenschwander, Pitts, 2019]. To ensure the highest vertical precision, strict filtering criteria were applied, considering the known sensitivity of the photon-counting LiDAR to solar background noise, canopy cover, and beam strength [Liu et al., 2021].

Ground-return selection. Only ground-classified photons from ATL08 were used for DEM validation, as these best represent the bare-earth surface required for DTM accuracy assessment. Ground photons were back-indexed to the ATL03 track data, preserving the sub-meter spatial resolution and geolocation accuracy. This approach follows standard practices in ICESat-2 terrain studies [Neuenschwander et al., 2020; Guenther et al., 2024].

Nighttime acquisition filtering. Because the Advanced Topographic Laser Altimeter System instrument is highly sensitive to solar background noise, only nighttime, strong-beam acquisitions were retained. Nighttime data provide a substantially higher signal-to-noise ratio, improving terrain detection under dense forest canopy [Liu et al., 2021; He et al., 2023]. Previous evaluations have shown that canopy-height RMSE decreases from 7.2 m to ≈3.9 m when limiting analyses to strong/night passes [Neuenschwander et al., 2020].

Final dataset. After applying all filters — signal-to-noise ratio >3, canopy height <1 m, beam=strong, and time=night — the dataset was comprised of more than 2 million ground-return photons across the study area.

This dense sampling yields a vertical precision better than 0.3 m RMSE, comparable to airborne LiDAR benchmarks, and enables spatially continuous mapping of DEM residuals in a forested mountain terrain.

Studied Digital Elevation Models (DEMs). Seven global DEMs were analyzed in this study: SRTM v3, NASADEM, ASTER GDEM v2, ALOS AW3D30, Copernicus GLO-30, FABDEM, and TanDEM-X. All datasets are primarily available at a 1 arc-second (~30 m) spatial resolution, except TanDEM-X, which also provides a finer 12 m version. These DEMs represent a mixture of optical stereo-photogrammetric and Synthetic Aperture Radar (SAR) — based products, and together they form the core set of elevation data used in modern hydrological, geomorphological, and flood modeling applications. Most of them are Digital Surface Models (DSMs), capturing the top reflective surface (vegetation and built structures), whereas FABDEM is an explicitly corrected DTM representing bare-earth elevation.

ASTER GDEM v2. The ASTER Global Digital Elevation Model v2 was generated photogrammetrically from along-track stereoscopic imagery captured by the ASTER aboard NASA's Terra satellite. Using nadir- and backward-looking telescopes in the near-infrared band, the system produced stereo pairs with a base-to-height ratio of 0.6. Released in 2011, version 2 incorporated ≈260 000 additional scenes compared to v1, improved geolocation, refined correlation algorithms (5×5 kernel), and enhanced water masking. It provides a near-global coverage between 83°N and 83°S at ~30 m resolution, with a typical vertical accuracy (LE90) of 15—20 m. While improved over v1, ASTER GDEM v2 still exhibits striping artifacts and canopy-induced elevation bias, performing best over bare terrain.

ALOS AW3D30. The ALOS World 3D 30 m (AW3D30) DEM was produced by the Japan Aerospace Exploration Agency using the PRISM sensor aboard ALOS, which acquired triplet stereo images (nadir, backward, forward) between 2006 and 2011 at a 2.5 m optical resolution. The global 30 m product is a resampled version of the original 5 m commercial dataset. Versions 3.1—3.2 improved void-filling and calibration, particularly at high latitudes. Validation against LiDAR indicates a vertical RMSE of ≈4.4 m, making AW3D30 one of the most accurate photogrammetric DEMs freely available.

Copernicus DEM (GLO-30). The Copernicus DEM GLO-30, distributed by the European Space Agency, is a refined, hydrologically edited DSM derived from WorldDEM™, which was produced from TanDEM-X X-band Interferometric Synthetic Aperture Radar (InSAR) data (2010—2015). The global 1 arc-second (~30 m) version was generated by resampling the original 12 m WorldDEM™ and performing extensive post-processing: void filling, water-body flattening, terrain structure correction, and hydrological conditioning using auxiliary datasets (ASTER GDEM, SRTM, GMTED2010, AW3D30, and national DEMs). The reported absolute vertical accuracy is ≈4 m (LE90). As a DSM, Copernicus DEM represents canopy and building tops, but its consistency and coverage make it highly suitable for continental-scale hydrological and geodetic analyses.

TanDEM-X (12 m/30 m). The TanDEM-X global DEM is based on X-band InSAR data acquired by twin satellites TerraSAR-X and TanDEM-X flying in close formation. The mission employed single-pass interferometry to derive a global DSM at a 12 m (0.4 arc-sec) resolution, later resampled to 30 m for general use. While TanDEM-X offers sub-meter relative accuracy in flat terrain, InSAR-specific distortions such as foreshortening, layover, and radar shadow can degrade elevation quality in steep or vegetated areas. Partial vegetation penetration of the X-band signal remains a known uncertainty source.

FABDEM (Forests and Buildings Removed Copernicus DEM v1.2). FABDEM is a 1 arc-second (~30 m) DTM derived from the Copernicus GLO-30 DSM (2011—2015) through machine-learning corrections. A Random Forest model trained on airborne LiDAR systematically removed elevation biases from vegetation and built-up structures, converting the DSM into a bare-earth representation. Validation shows FABDEM reduces mean absolute vertical error by roughly half relative to its parent model — ≈1.1 m in urban and ≈2.9 m in forested areas — making it the most accurate freely available global DTM. The dataset is distributed for non-commercial scientific use.

SRTM DEM v3. The Shuttle Radar Topography Mission (SRTM) DEM originates from C-band InSAR data collected during an 11-day space-shuttle mission in February 2000. Initially providing a 1 arc-second (~30 m) coverage only for the U.S., later releases expanded global availability. The void-filled SRTM v3 («SRTM Plus»), released in 2014—2015, filled gaps using auxiliary datasets such as ASTER GDEM. Reported vertical accuracy ranges from 4 to 16 m (RMSE), depending on terrain complexity. SRTM remains one of the most widely used baseline datasets for regional hydrological modeling.

NASADEM v1 released in 2020, is a complete reprocessing of the original SRTM C-band data using improved SAR calibration, orbit modeling, and auxiliary inputs from ASTER, ICESat, and GLAS altimetry. It eliminates remaining voids and systematic artifacts (e.g., antenna boom motion «ripples»), yielding enhanced vertical precision and global consistency. NASADEM is intended as the successor to SRTM, maintaining the same 30 m resolution while improving elevation continuity and geolocation accuracy. Although large-scale independent validation is ongoing, preliminary assessments show a measurable reduction in RMSE compared to SRTM v3.

The analyzed DEMs collectively represent the evolution of global elevation mapping — from early space-borne radar missions (SRTM) to high-precision interferometric (TanDEM-X, Copernicus) and machine-learning-enhanced terrain products (FABDEM).

Their diverse sensing principles and pro-

cessing chains determine suitability for specific hydrological applications, from floodplain delineation to geomorphometric analysis.

Vertical Transformation. To ensure vertical consistency across transboundary and mountainous regions, all elevation datasets used in this study were transformed from their original vertical datums (e.g., EGM96, EGM2008) to the EGG2015 is the latest high-precision quasi-geoid model for Europe and represents the official realization of the European Vertical Reference System (EVRS) through EVRF2007 [Denker, 2015; Denker et al., 2018]. Compared with earlier versions (EGG97, EGG2008), it integrates densified terrestrial gravity data, the Gravity field and steady-state Ocean Circulation Explorer — based geopotential model GOCO05S, and regional refinements, achieving sub-decimeter accuracy across most of Europe.

Validation studies demonstrate the exceptional reliability of EGG2015. Across Central Europe, mean residuals between EGG2015 and Global Navigation Satellite System levelling data are typically below 2 cm, confirming its suitability for high-accuracy vertical transformations [Denker, 2015]. Regional evaluations in Western Ukraine reported residuals of about 7 cm [Zablotskyi et al., 2021], while studies in Poland [Marjańska et al., 2019] showed consistency with the European Terrestrial Reference Frame 2000 (ETRF2000) frame at 1.3—2.0 cm RMSE after surface-fitting adjustments. Together, these results confirm that EGG2015 represents the most accurate continental-scale gravimetric quasi-geoid currently available.

Therefore, all DEMs were harmonized to EGG2015 using the licensed 1′×1′ height-anomaly grid provided by Prof. H. Denker (Leibniz University Hannover, Germany). This full-resolution dataset is not part of the public International Service for the Geoid release (the public grid has 10′×15′ spacing; [Denker, 2015], DRCI: DATA2018076013172051) but ensures compatibility with the Geodetic Reference System 1980 (GRS80) ellipsoid, the zero-tide system, and the EVRF2007 vertical reference frame.

This configuration guarantees compliance with the INSPIRE and EU Floods Directive requirements and enables consistent comparison with ICESat-2 elevations:

$$H=h-N,$$

where H is the orthometric (gravity-related) height, h the ellipsoidal height (WGS-84), and N the geoid height anomaly derived from the licensed EGG2015 grid. This transformation ensured a physically consistent gravity-related reference system for all DEMs and ICESat-2 points.

Accuracy Assessment Metrics. To evaluate the vertical accuracy of the analyzed DEMs, we applied a set of classical and robust statistical metrics using ICESat-2 ATL08 elevations as the reference dataset. Classical point-based indicators included the ME, RMSE, and MAE, which quantify systematic bias and total elevation deviation:

$$\mathrm{ME}=\frac{1}{n}\sum_{i=1}^{n}\left(Z_{\mathrm{DEM}_i}-Z_{\mathrm{ref}_i}\right),$$

$$\mathrm{RMSE}=\sqrt{\frac{1}{n}\sum_{i=1}^{n}\left(Z_{\mathrm{DEM}_i}-Z_{\mathrm{ref}_i}\right)^2},$$

$$\mathrm{MAE}=\frac{1}{n}\sum_{i=1}^{n}\left|Z_{\mathrm{DEM}_i}-Z_{\mathrm{ref}_i}\right|.$$

where $Z_{\mathrm{DEM}i}$ and $Z_{\mathrm{ref}i}$ are the DEM and ICESat-2 elevations, respectively, and n is the number of collocated samples.

These metrics provide global measures of DEM performance but are sensitive to outliers and non-Gaussian error distributions [Mesa-Mingorance, Ariza-López, 2020].

To account for non-normal error behavior and local variability, we additionally computed the NMAD [Höhle, Höhle, 2009]:

$$\mathrm{NMAD}=1.4826\times$$
$$\times\mathrm{median}\left(\left|Z_{\mathrm{DEM}_i}-Z_{\mathrm{ref}_i}-\mathrm{median}\left(Z_{\mathrm{DEM}}-Z_{\mathrm{ref}}\right)\right|\right)$$

as NMAD offers a robust estimate of vertical dispersion that is less affected by extreme residuals. By mapping NMAD across geomorphological (slope, landform), hydrological (HAND, TWI), and land-use and land-cover (LULC) gradients, we quantified how terrain complexity and surface properties control DEM uncertainty. This combined use of

RMSE, MAE, ME, and NMAD provides a comprehensive assessment of DEM accuracy, bias, and robustness across diverse physiographic settings.

Dashboard-based data processing. All analyses were implemented within the GeoHydroAI framework, built on Python 3.11, GDAL, Dash, and DuckDB.

The environment integrates GDAL for raster and vector data handling, Rasterio and PyProj for projection management, xDEM and WhiteboxTools for terrain and hydrological analysis, and the SlideRule ICESat-2 API for satellite altimetry retrieval. The interactive Dash dashboard connects these components, enabling filtering, aggregation, and visualization of large geospatial datasets through DuckDB SQL queries. This architecture ensures computational efficiency, reproducibility, and seamless integration between the low-level GDAL operations and the high-level analytical visualization.

Satellite altimetry points (ATL03/ATL08) were retrieved directly from NASA's SlideRule server (slideruleearth.io) using the official Python client, enabling selective downloading of photons within the study area and automatic conversion into geospatial layers. Derived terrain parameters — including slope, flow accumulation, Topographic Wetness Index (TWI), HAND, and geomorphons — were computed using WhiteboxTools, while vertical transformations and DEM differencing were performed with xDEM.

LULC data were incorporated from Copernicus Global Land Service and ESRI 10-m LULC maps, resampled to match the DEM resolution and spatial reference.

This integration allowed cross-analysis between topographic variables and surface characteristics, improving the interpretation of terrain-dependent discrepancies in satellite altimetry.

All raster and vector datasets were stored in optimized Parquet/GeoParquet formats, ensuring efficient access through DuckDB.

The dashboard supports dynamic filtering by sub-basins, slope ranges, HAND classes, geomorphic forms, or LULC categories, linking analytical plots with interactive map visualizations. This integrated workflow bridges classical terrain analysis based on Geographic Information Systems with modern data-driven hydrological modeling, providing a transparent, reproducible, and computationally efficient framework for multi-source elevation accuracy assessment.

The integrated GeoHydroAI [GeoHydroAI, 2025] framework enabled a unified and reproducible evaluation of DEM accuracy and hydrological reliability across multiple spatial dimensions. By combining classical accuracy indicators (ME, MAE, RMSE) with the robust NMAD metric, the analysis captured both systematic and distribution-based components of elevation uncertainty.

Coupling these quantitative assessments with an interactive analytical dashboard allowed dynamic visualization and instant feedback on how DEM residuals respond to variations in slope, land cover, and hydrological position. The following section presents the results of this assessment, emphasizing spatial error patterns, vertical-accuracy gradients, and their implications for floodplain modeling in the Ukrainian Carpathians.

Results. ***Vertical accuracy assessment.*** This section presents the validation results of the seven global DEMs against ICESat-2 elevations referenced to the EGG2015 vertical datum. The analysis is spatially stratified across geomorphological, land-cover, and hydrological gradients. Fig. 2—5 summarize classical error metrics — RMSE, MAE, ME, and NMAD — and demonstrate their variability under different terrain and surface conditions.

Fig. 2 shows the RMSE distribution across terrain types (valleys and slopes), land-cover classes (trees, built-up areas, water), and hydrological settings (HAND 0—6 m). FABDEM exhibits the lowest RMSE values (6.41 m overall; 2.11 m in low-relief built-up areas), whereas ASTER displays the highest errors (up to 16.38 m in forested terrain). RMSE increases with slope and vegetation density.

Fig. 3 presents MAE across the same spatial filters. FABDEM yields the lowest MAE in most conditions (1.42—1.56 m in built-up areas), while ASTER and ALOS reach high

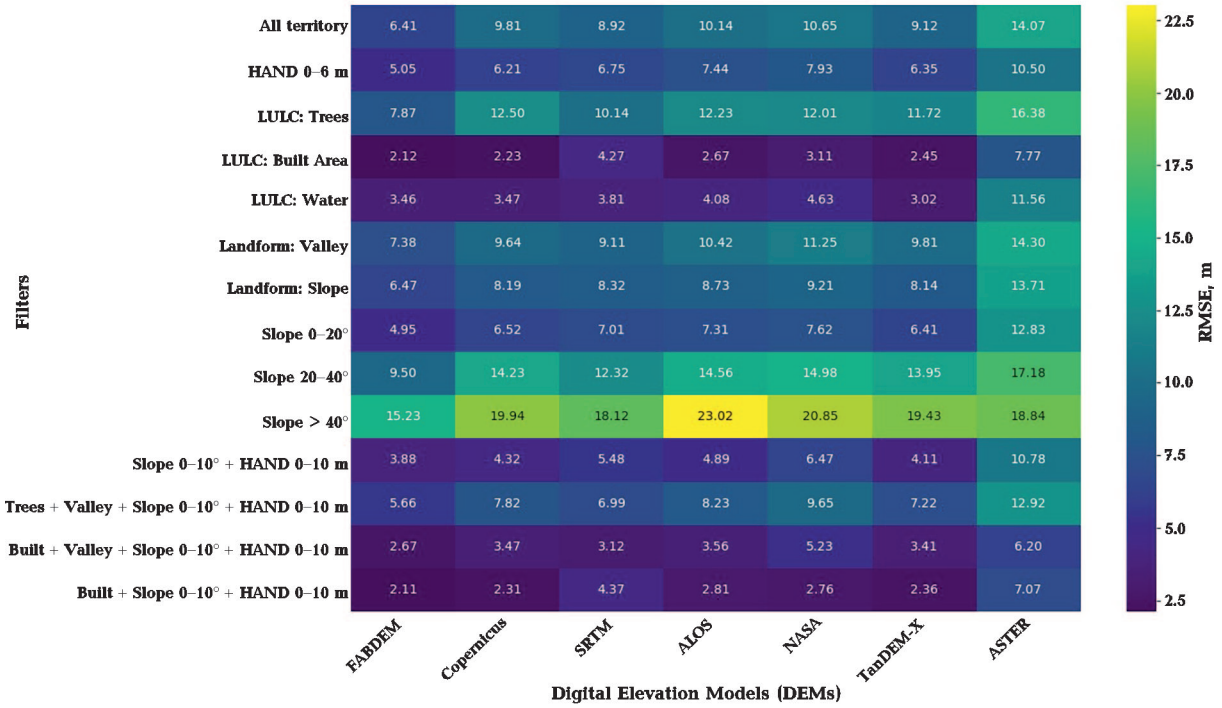

Fig. 2. Root Mean Square Error (RMSE, m) of seven global DEMs across terrain (valley and slopes), land cover (trees, built area, water), and hydrological HAND filters. «HAND 0—6 m» zone represents all areas with height above the nearest drainage channel (riverbed) between 0 and 6 meters.

deviations on steep slopes (up to 21.83 m). Across all DEMs, MAE increases with slope and canopy cover and remains smallest in flat and built-up zones.

Fig. 4 summarizes systematic vertical bias (ME). Most DEMs show a positive bias (overestimation of surface elevation), particularly in steep terrain (up to +11.03 m for ALOS at slopes >40°). FABDEM and Copernicus DEM display the smallest bias values. ASTER occasionally produces negative bias in built-up areas (–5.29 m).

Fig. 5 presents NMAD as a distribution-robust metric across hydrological and geomorphological gradients:

– TWI: NMAD decreases at higher wetness values;

– HAND: NMAD increases with distance above drainage; errors are minimal in floodplain zones (HAND <2 m);

– Landforms: Peaks, ridges, and valleys exhibit higher NMAD, whereas footslopes remain relatively stable;

– Slope: NMAD increases nonlinearly with steepness, from ~3 m in flat terrain (0—2°) to >10 m in slopes >12°;– LULC: Tree-covered areas show the highest NMAD (>10 m), while developed and water surfaces remain lowest (<4 m).

Across all gradients, FABDEM produces the smallest NMAD values (typically <5 m), while ASTER and ALOS exhibit the highest values in complex topography.

HAND and TWI exhibit an inverse relationship (r≈–0.8), and their combined gradients explain the variance of errors across drainage-proximal and slope-dominated zones. NMAD increases with HAND (>9 m above 20 m) and decreases in wet, low-lying areas (NMAD ~3 m). Vegetated surfaces consistently produce the largest NMAD across all DEMs.

Cross-section-based assessment. Fig. 6—8 evaluate the vertical consistency of DEM-derived riverbed profiles relative to the surveyed reference cross-section at Yablunytsia (*H*=597.815 m EVRS; spacing=2 m).

Fig. 6 shows the DEM-sampled bed elevations relative to the reference. ASTER shows a deeper thalweg, while radar-derived

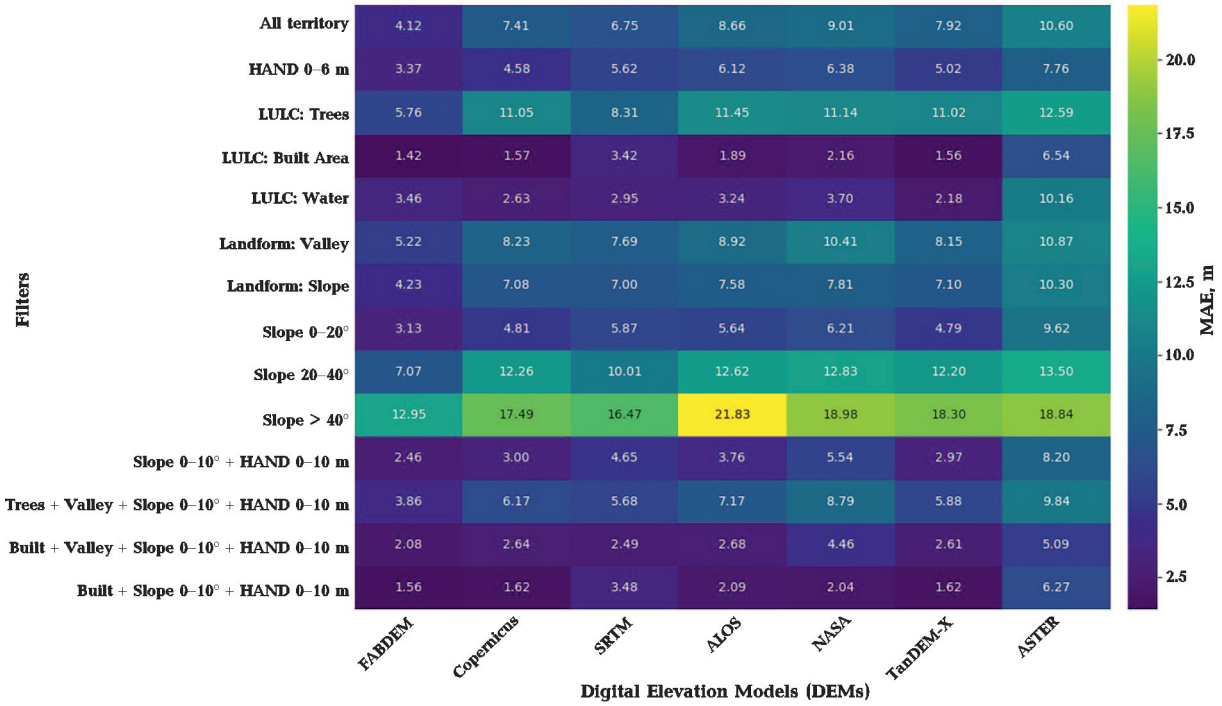

Fig. 3. Mean Absolute Error (MAE, m) of seven global DEMs across geomorphological, hydrological, and land-cover filters.

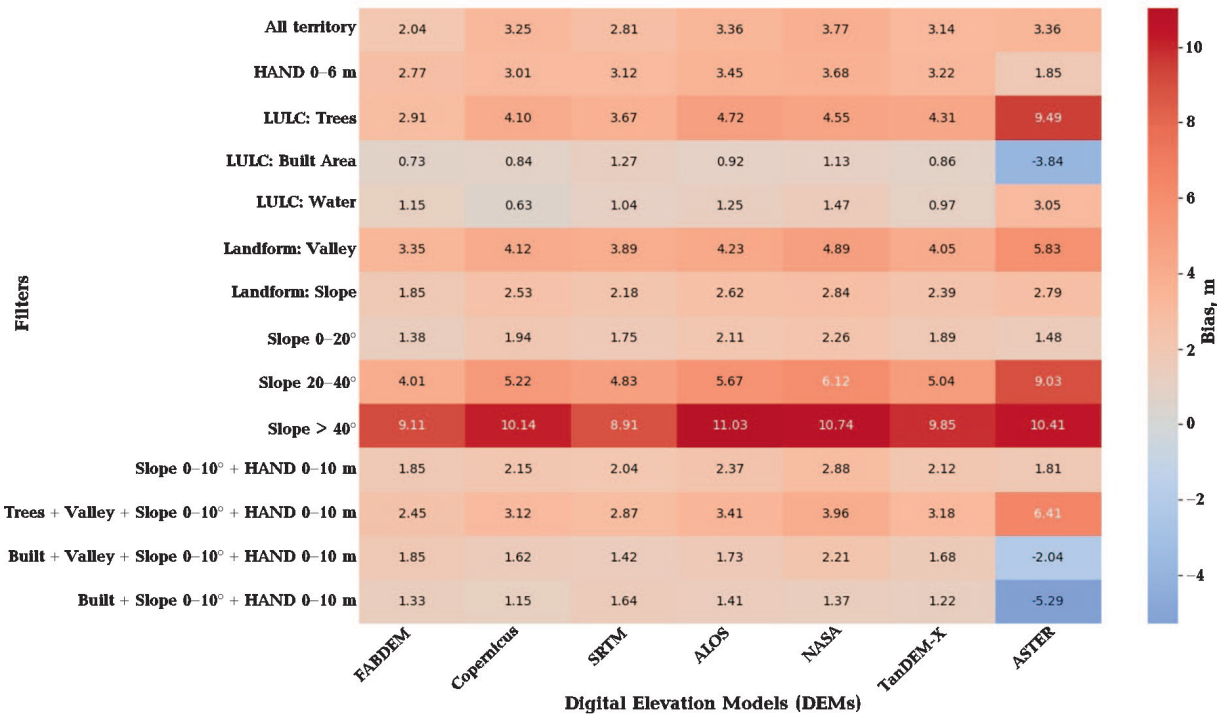

Fig. 4. Systematic vertical bias (m) of global DEMs across geomorphological, hydrological, and land-cover filters.

DEMs (SRTM, TanDEM-X, ALOS) and FABDEM produce higher-than-actual bed elevations. NASADEM does not form a wetted cross-section at the given water level.

Fig. 7 presents water-depth estimates computed as depth=max(H–bed, 0). The reference

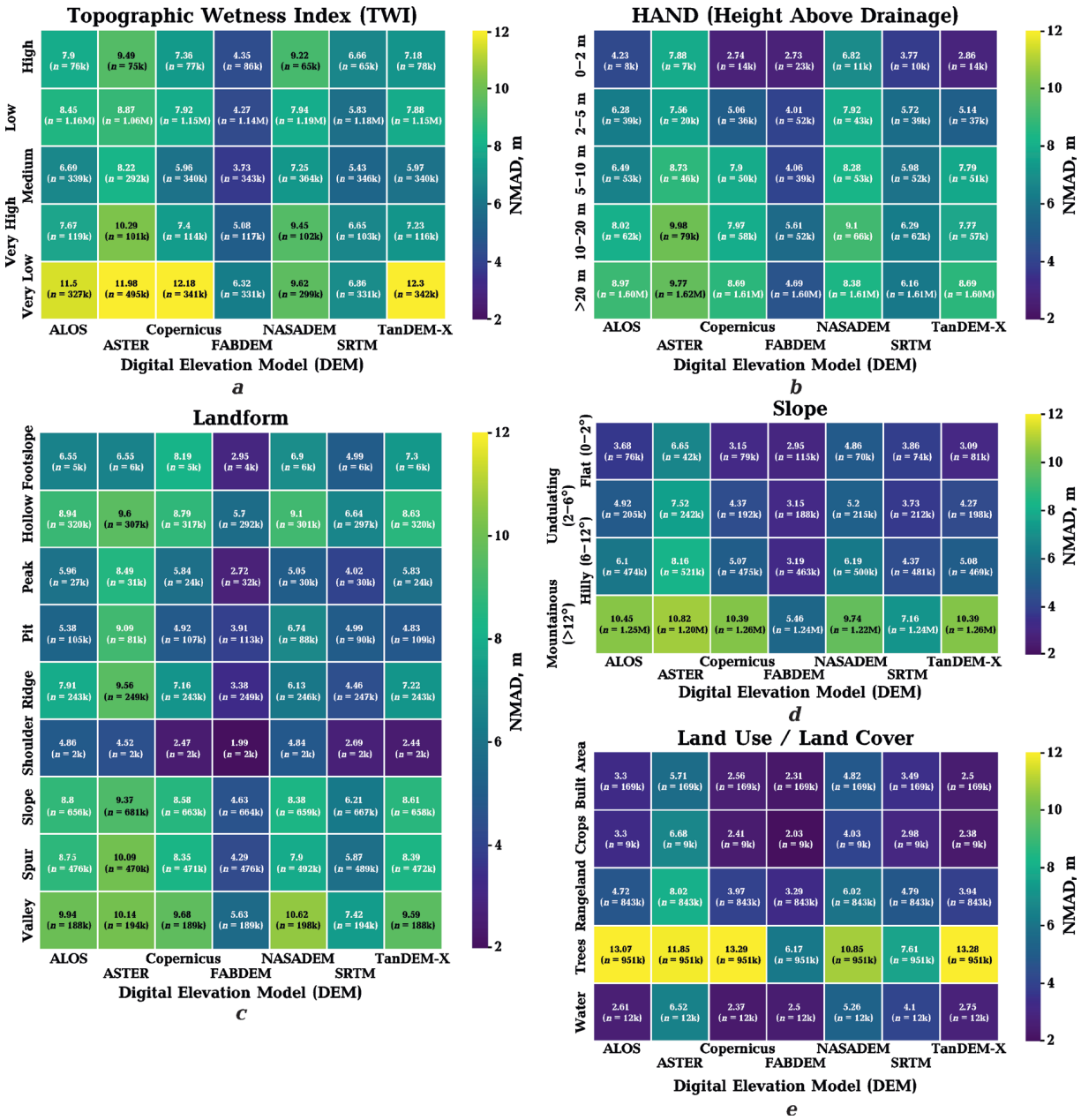

Fig. 5. Normalized Median Absolute Deviation (NMAD, m) of global DEMs across hydrological and geomorphological gradients TWI (*a*); HAND (*b*); Landform classification (*c*); Slope classes (*d*); LULC (*e*).

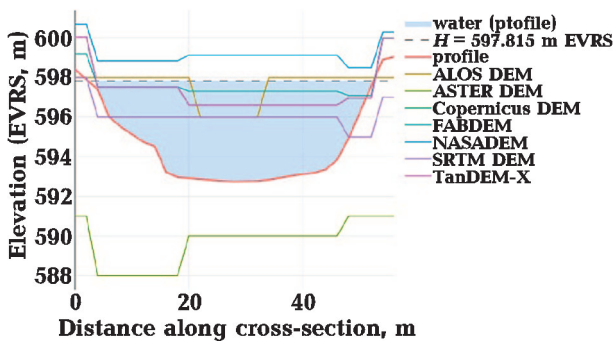

Fig. 6. Cross-section bed profiles (reference+DEMs) at *H*=597.815 EVRS.

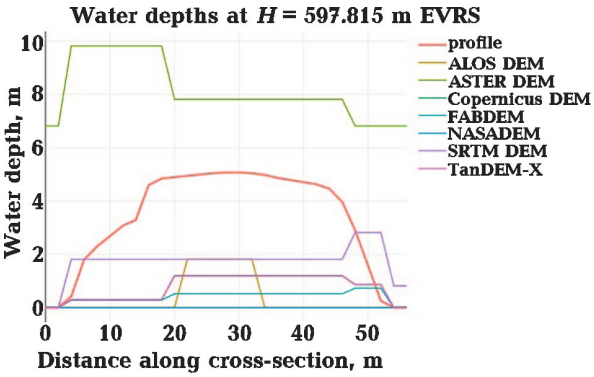

Fig. 7. Water-depth profiles at *H*=597.815 m (EVRS).

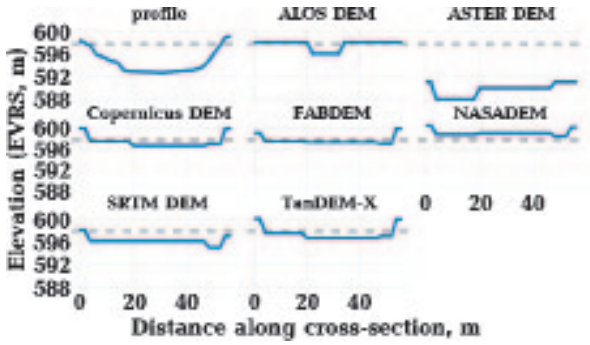

Fig. 8. Individual DEM cross-section profiles at *H*=597.815 m (EVRS).

profile shows 3—5 m depths. ASTER produces depths of 8—10 m, while Copernicus/TanDEM/ALOS/FABDEM/SRTM underestimate depths (<2 m across long segments). NASADEM yields zero depth.

Fig. 8 shows each DEM cross-section individually, highlighting the characteristic vertical deviations:

– ASTER: deeper bed;

– Copernicus, TanDEM-X, FABDEM, ALOS, SRTM: elevated beds and reduced depths;

– NASADEM: no wetted section.

Table 2 summarizes wetted-section metrics (A, P, W, $\bar{D}$, R) and their deviations from the reference cross-section (A=190.361 m^2, P=52.266 m). Positive ΔA indicates overestimation, while negative values indicate underestimation relative to the surveyed reference.

Results indicate:

– ASTER: strong overestimation of wetted area (+267.279 m^2; +140.41 %);

– SRTM: moderate underestimation (–91.166 m^2; –47.89 %);

– Copernicus, TanDEM-X, FABDEM, ALOS: substantial underestimation (–147 to –169 m^2; –77 to –89 %);

– NASADEM: no wetted section detected (A=0 m^2).

Regulatory accuracy context. Fig. 9 compares DEM RMSE across slope classes with INSPIRE Recommendation 52, Table 7 (European Commission, 2013). For 30 m DEMs, the admissible RMSE range is 1.5—10 m in flat/undulating terrain (0—6°) and 3—10 m in hilly/mountainous terrain (>6°). Most DEMs

Table 2. Wetted cross-section metrics and their deviations from the surveyed reference cross-section at Yablunytsia (H=597.815 m EVRS; transverse spacing=2 m)

Wetted-section metrics and errors vs reference								
Profile	*A*, m^2	*P*, m	*W*, m	$\bar{D}$, m	*R*, m	Δ*A*, m^2	Δ*P*, m	Δ*A*, %
Reference cross-section	190.361	52.266	52.000	3.661	3.642	0.000	0.000	0.00
SRTM DEM	99.195	55.631	54.000	1.837	1.783	–91.166	3.365	–47.89
TanDEM-X	43.327	49.631	52.000	0.833	0.873	–147.035	–2.636	–77.24
Copernicus DEM	43.235	49.626	52.000	0.831	0.871	–147.126	–2.640	–77.29
FABDEM	23.423	49.357	52.000	0.450	0.475	–166.938	–2.909	–87.70
ALOS DEM	21.780	15.134	14.000	1.556	1.439	–168.581	–37.133	–88.56
NASADEM	0.000	0.000	0.000	0.000	0.000	–190.361	–52.266	–100.00
ASTER DEM	457.640	58.670	56.000	8.172	7.800	267.279	6.404	140.41

Notes: A — wetted area, *P* — wetted perimeter, *W* — water surface width, $\bar{D}$ — mean depth, *R* — hydraulic radius. Cell colors indicate the direction of deviation from the reference cross-section: red denotes negative deviations (underestimation of parameters), while green denotes positive deviations (overestimation).

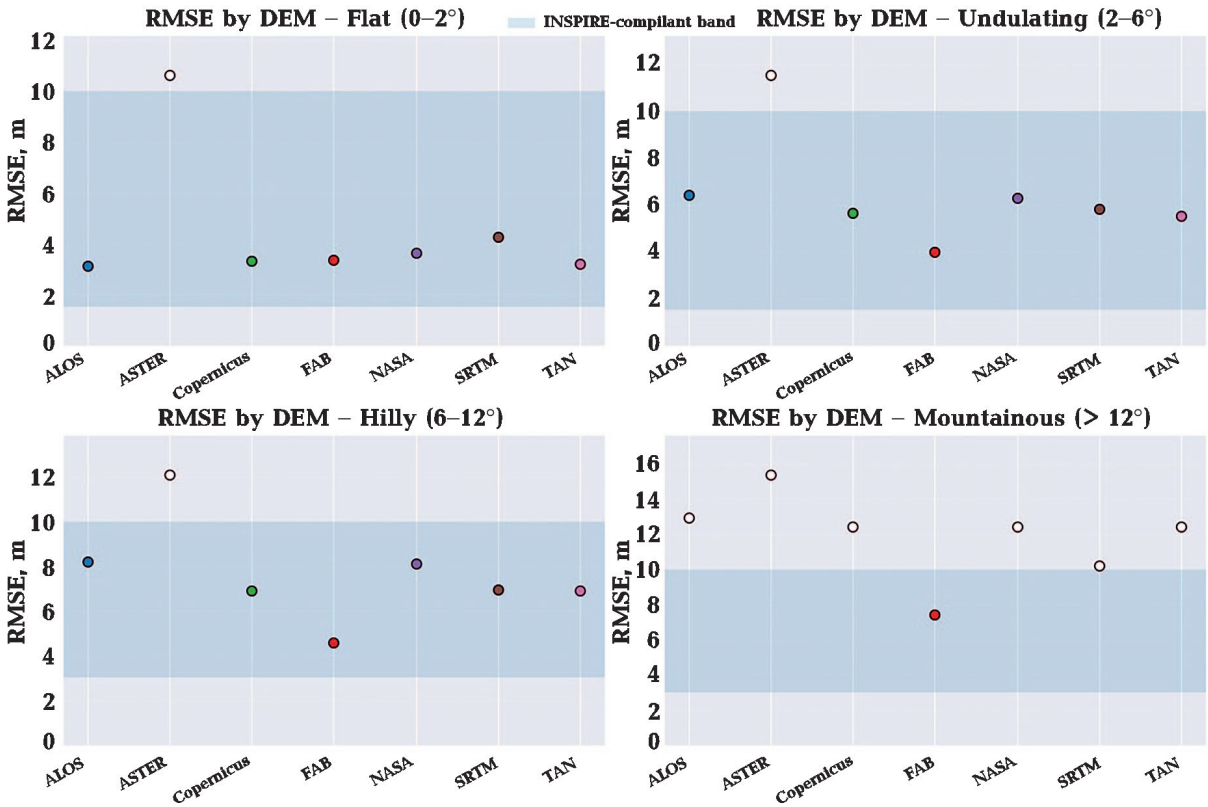

Fig. 9. RMSE of global DEMs across slope classes compared to the compliance bands defined in INSPIRE Recommendation 52, Table 7 (European Commission, 2013).

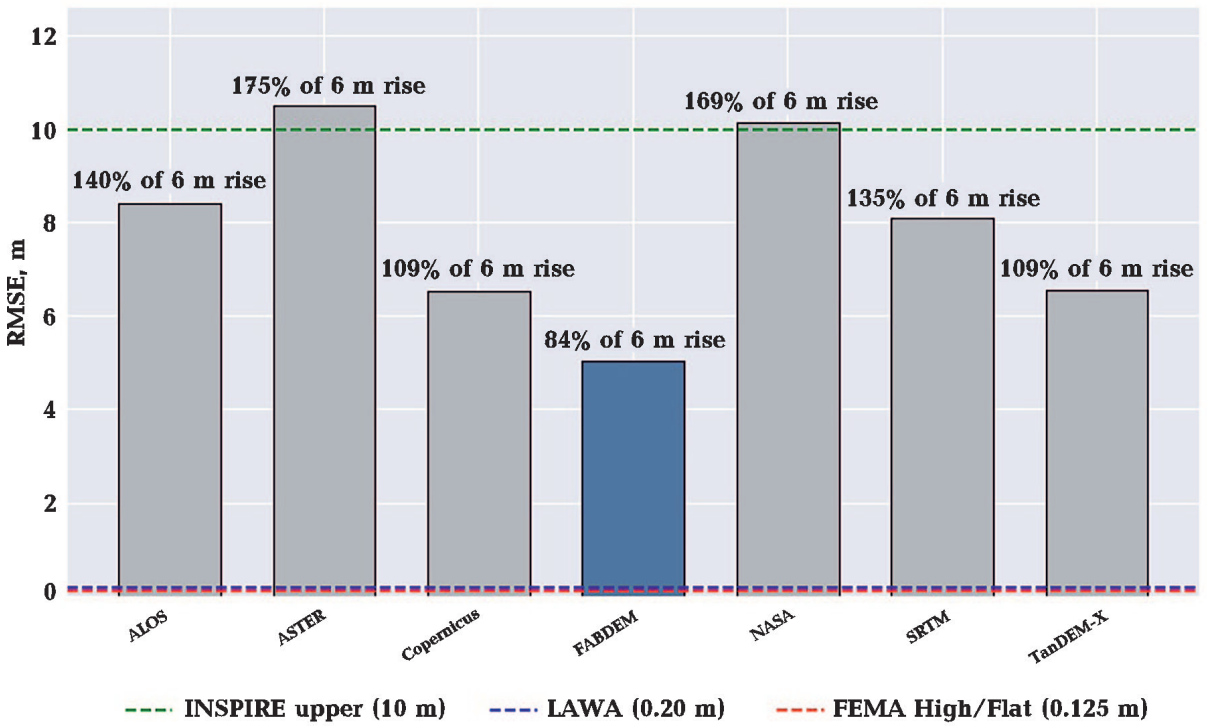

Fig. 10. Floodplain band selection and regulatory context (HAND 0—6 m).

comply under low-relief conditions; in mountainous terrain only FABDEM remains within INSPIRE bounds.

Fig. 10 evaluates RMSE within the HAND 0—6 m band. Dashed lines represent INSPIRE (10 m), LAWA (0.20 m), and FEMA High/Flat (0.125 m) reference limits. RMSE values are additionally normalized by the 6 m HAND rise (RMSE/6×100 %). FABDEM shows the lowest errors within this hydrologically relevant zone.

Floodplain mapping sensitivity. Fig. 11 shows comparative HAND 5 m flood-zone delineations derived from ASTER (red) and FABDEM (blue). Differences illustrate sensitivity of HAND-based flood mapping to DEM vertical accuracy. (Interactive version provided as Supplementary Material S1.)

Fig. 12 shows static HAND 5 m flood-zone comparisons between SRTM (blue gradient) and Copernicus DEM (red gradient). Despite using the same hydrological reference, SRTM produces wider flood extents, whereas Copernicus DEM generates smoother and more spatially coherent flood boundaries.

Discussion. ***Drivers of Vertical Error Across Global DEMs.*** The comparative evaluation of seven global DEMs reveals consistent performance patterns that align with both the underlying sensing technologies and established terrain-error relationships. Across all spatial filters — slope, land cover, HAND, and TWI — vertical accuracy decreases systematically with increasing terrain steepness and vegetation density. These trends are well-documented in prior global assessments of radar- and optical-derived DEMs [Carabajal, Harding, 2006; Liu et al., 2019; Hawker et al., 2019 ; Han et al., 2024; Meadows et al., 2024].

Steep slopes amplify vertical error due to a combination of geometric distortions, horizontal offsets, and radar layover/shadowing [Rizzoli et al., 2017] Our results confirm this non-linear trend, with RMSE and NMAD increasing from <4 m in flat terrain to >10—20 m in highly sloped regions. Vegetation introduces an additional structural bias: radar sensors measure canopy top surfaces rather than the ground, and optical stereo methods suffer from texture variations and occlusion [Baugh et al., 2013; Li et al., 2022]. Forested pixels consistently exhibited the largest errors across all DEMs, in agreement with global findings.

The inverse relationship between HAND and TWI ($r \approx -0.8$) further explains spatial

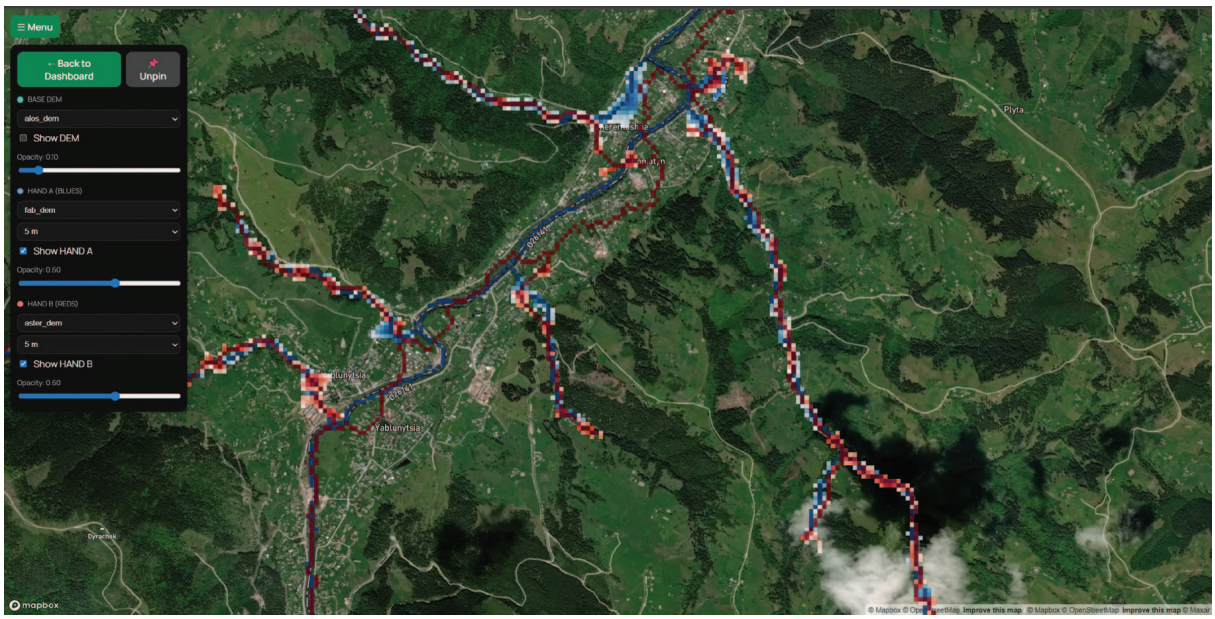

Fig. 11. Comparative HAND flood zones derived from different DEMs (interactive dashboard view). Blue pixels show the HAND flood zone calculated from DEM 1, and red pixels show the HAND flood zone calculated from DEM 2. Since the HAND level is the same, the differences reflect only how each DEM represents elevation.

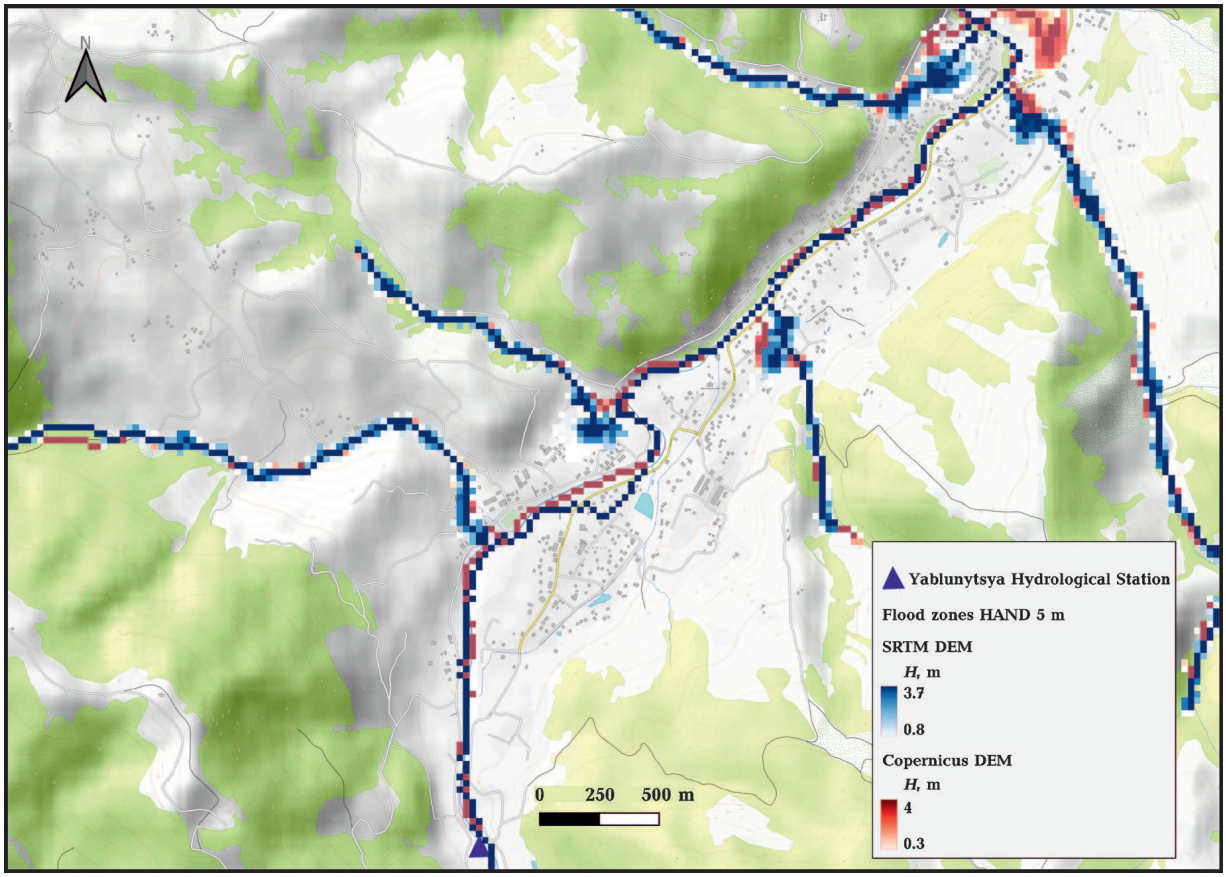

Fig. 12. Static map comparison of HAND 5 m flood zones for the Yablunytsia reach derived from multiple DEM products. Base map: OpenTopoMap © OpenStreetMap contributors. Projection: WGS84 (EPSG:4326).

patterns in error magnitude. The low-HAND areas — corresponding to floodplains and terrain depressions – exhibit both high moisture and low slope, which reduce DEM uncertainty. Conversely, zones >20 m above drainage combine increased slope, microtopographic roughness, and low moisture, driving error growth. This joint HAND-TWI behavior has been observed in DEM uncertainty propagation in floodplain studies [Sampson et al., 2016; Hawker et al., 2022].

DEM structural properties: DSM versus DTM behavior. A central finding of this study is the systematic distinction between DEMs functioning effectively as DSMs versus DTMs. Copernicus DEM, TanDEM-X, ALOS, SRTM, ASTER, and NASADEM all behave as DSMs, retaining vegetation and developed-surface artefacts to varying degrees. The positive elevation bias observed across the developed and forested zones is consistent with this behavior and aligns with previous analyses demonstrating incomplete canopy/structure penetration by radar and optical systems [Hirt et al., 2010; Gesch, 2018; Uuemaa et al., 2020; Guth et al., 2021].

FABDEM was the only DEM consistently functioning as a DTM across geomorphological classes. Its lower error statistics reflect the machine-learning-based filtering of Copernicus DEM aimed at removing vegetation and anthropogenic structures [Hawker et al., 2022]. The dataset maintained superior accuracy across slope, HAND, and LULC classes, particularly in steep terrain, where DSM-related biases were amplified in other DEMs.

These distinctions are not only relevant from a remote-sensing perspective but are critical for hydrological applications. DSMs tend to elevate valley floors («digital dams»), create spurious obstructions, and distort flow pathways [Duke et al., 2003; Neal et al., 2009;

Sampson et al., 2016; Hawker et al., 2022], whereas DTMs preserve channel hydraulics more faithfully.

Propagation of DEM uncertainty into hydraulic geometry. The cross-section assessment at the Yablunytsia gauging station provides a clear demonstration of how structural DEM errors propagate into hydraulic model parameters. DSM-type DEMs (Copernicus, TanDEM-X, ALOS, SRTM) produced wetted-area underestimations between 48 and 89 % at a fixed water stage. The elevated bed surfaces observed in these datasets directly reduce depth and hydraulic radius, artificially increasing roughness and reducing conveyance.

NASADEM represents an extreme DSM-like failure case: the DEM could not generate a wetted polygon at the reference stage, consistent with known issues of radar backscatter saturation in narrow valleys [Rodriguez et al., 2006]. In hydraulic models, such distortions cause abrupt discontinuities in water-surface profiles and can generate non-physical backwater effects.

ASTER exhibited the opposite behavior — over-deepening the channel — consistent with optical stereo artefacts creating pits, spikes, and unrealistically low thalweg elevations [Farooq et al., 2019]. This led to wetted-area overestimation of +140 %, demonstrating that vertical errors can produce both false attenuation and false amplification of flow capacity.

Overall, the cross-section experiment shows that DEM errors are not random noise but structural distortions that propagate directly into the hydraulic terms A, P, W, $\overline{D}$, and R, which in turn control shear stress, velocity, and discharge.

Regulatory thresholds and implications for flood modeling. The regulatory comparison (INSPIRE, LAWA, FEMA) underscores the performance gap between global DEMs and terrain standards required for high-precision flood hazard mapping. While most DEMs satisfy INSPIRE RMSE requirements in flat terrain, only FABDEM remains within acceptable limits in mountainous terrain (>6°). In the HAND 0—6 m floodplain band, RMSE values from 5 to 10 m correspond to 84—175 % of the 6 m observed flood-rise margin. This means that DEM vertical uncertainty is of the same magnitude — or greater — than the flood depth being modelled.

Such conditions make regulatory-grade inundation delineation infeasible. This agrees with earlier studies showing that global DEM-based flood maps systematically shift flood boundaries upslope and overestimate inundation width in steep valleys [Hawker et al., 2018; Uuemaa et al., 2020].

At the same time, global DEMs retain practical value for regional flood screening and exploratory scenario analysis — especially in settings lacking LiDAR coverage, such as Ukraine. The key is acknowledging that these datasets cannot be used for detailed hydraulic modelling, flood zoning, or engineering design.

Vertical referencing and the importance of geodetic consistency. The harmonization of all DEMs and ICESat-2 altimetry to the EGG2015 quasi-geoid significantly reduced vertical inconsistencies across datasets. Vertical datums remain a major source of hidden bias in hydrological modelling, particularly across national boundaries or mountainous terrain [Afrasteh et al., 2023]. Our results highlight that proper referencing can eliminate systematic offsets of tens of centimeters — small relative to the metre-scale DEM errors, but critical for distributed hydrological modelling, especially in floodplains where gradients are low.

The success of international projects such as Danube Floodrisk demonstrates that high-quality, cross-border flood modelling requires harmonized vertical reference systems. The lack of EVRS-aligned LiDAR data in Ukraine therefore remains a key limitation for regulatory flood mapping in transboundary basins.

Implications for Carpathian flood modelling and data selection. Based on the combined results, several practical implications emerge:

1. FABDEM, which represents a machine-learning-corrected DTM with vegetation and buildings removed, is the most appropriate DEM for hydrological and hydraulic model-

ling in the Carpathians, outperforming the analyzed DSMs across slope, land-cover, and HAND classes. This lower bias is therefore primarily attributable to surface-type differences (DTM versus DSM), rather than to intrinsic sensor accuracy.

2. DSM-type DEMs should not be used for hydraulic modelling because they systematically distort channel geometry and wetted cross-sections.

3. Floodplain analyses using HAND are highly sensitive to vertical bias, especially in steep and narrow valleys.

4. Copernicus DEM remains suitable for regional exposure mapping, but not for detailed hydraulic modelling due to its DSM character and insufficient grid–accuracy consistency.

5. LiDAR is required for regulatory use, as no global DEM satisfies the LAWA/FEMA thresholds.

These results establish a consistent decision-making framework for DEM selection in mountainous basins of Central and Eastern Europe lacking airborne LiDAR coverage.

Limitation of independent flood validation. It should be noted that the HAND-based floodplain comparison presented here represents a sensitivity analysis rather than an independent validation. Sentinel-1 GRD imagery was processed using standard radiometric calibration, terrain correction, and threshold-based water classification workflows; however, reliable flood masks could not be obtained for the investigated mountainous catchments. Backscatter separability between inundated and non-inundated pixels was insufficient due to radar shadowing, layover effects, dense forest canopy, and sub-pixel channel widths characteristic of narrow mountain valleys. Consequently, SAR-derived flood extents exhibited high spatial uncertainty and were unsuitable as ground-truth references. Therefore, the HAND-based analysis should be interpreted as quantifying DEM-driven uncertainty propagation rather than absolute flood-extent accuracy.

Cartographic flood-inundation boundaries were not available for the investigated hydrological station. Historical records contain only longitudinal water-level profiles and discharge measurements, without mapped inundation extents. The available cross-section profile was incorporated into the manuscript for geometric sensitivity analysis; however, it does not allow spatial validation of floodplain polygons derived from HAND.

Conclusions and Implications. This study provides a comprehensive evaluation of the vertical accuracy and structural behavior of seven freely available global DEMs in the Ukrainian Carpathians. By harmonizing all elevation data to the EGG2015 quasi-geoid and validating them against the ICESat-2 ATL03/ATL08 altimetry, we established a consistent reference framework that removes datum-related offsets and isolates true DEM uncertainty.

Across the region, terrain slope and vegetation cover emerged as the primary controls on DEM error magnitude. Steep and forested landscapes produced the largest deviations, confirming widely documented limitations of radar and optical sensors in complex mountainous environments. Most DEMs — functioning effectively as DSMs — satisfied INSPIRE Recommendation 52 vertical-accuracy thresholds only in flat and undulating terrain, while errors in mountainous areas exceeded admissible limits by a factor of two to three.

These findings have direct implications for hydrological and hydraulic modelling. In the hydrologically critical HAND 0—6 m floodplain zone, DEM errors of 5—10 m propagate into substantial biases in inundation extent, depth, wetted area, and hydraulic radius. The results from the cross-section experiment at Yablunytsia demonstrate that DSM-type DEMs systematically distort channel geometry, suppressing depth and conveyance, while ASTER frequently exaggerates depth due to optical-stereo artefacts. Such distortions make regulatory-grade flood mapping infeasible with global DEMs.

Among the evaluated datasets, FABDEM consistently achieved the highest accuracy and was the only DEM that behaved as a true bare-earth DTM across geomorphological and hydrological gradients. Its performance underscores the necessity of using DTM-type datasets — rather than uncorrected DSMs

— for applications requiring precise water-surface modelling, floodplain delineation, or hydraulic routing.

It should be emphasized that the superior performance of FABDEM primarily reflects its DTM character achieved through machine-learning-based vegetation removal, whereas the remaining datasets behave as DSMs; thus, part of the observed accuracy contrast originates from surface-type differences rather than intrinsic DEM sensor performance.

It should be noted that the HAND-based floodplain comparison presented here represents a sensitivity analysis rather than an independent validation. No direct comparison with observed flood extents or hydrometric records was performed. Therefore, the reported differences quantify the propagation of DEM-related uncertainty into floodplain delineation, rather than the absolute predictive performance of individual models.

In a broader sense, this study establishes a regional benchmark for DEM selection, preprocessing, and uncertainty communication in mountainous catchments. The openly released results and interactive analyses provided through the GeoHydroAI DEM Dashboard [GeoHydroAI, 2025] support transparency, reproducibility, and cross-border harmonization under the EU Floods Directive (2007/60/EC). These resources can inform national and transboundary flood-risk assessments, particularly in regions lacking LiDAR-based national elevation models.

Future work will integrate Sentinel-1 flood-extent observations where physically feasible, calibrate hydrodynamic roughness using in situ and remote-sensing data, and apply probabilistic uncertainty propagation to quantify how DEM errors affect both steady-state and unsteady flow simulations. Together, these advances will contribute to more robust, harmonized, and data-driven flood-risk assessments across Central and Eastern Europe.

The present study represents the initial remote-sensing-based assessment phase of the broader GeoHydroAI project. A subsequent stage, supported by the Deutsche Bundesstiftung Umwelt, will integrate centimeter-level Global Navigation Satellite System Real-Time Kinematic Surveys to obtain precise channel and floodplain geometry in representative Carpathian river sections. These ground-truth measurements will enable the construction of hydraulically consistent 2D models and provide independent validation of flood extent and depth under real-event conditions. This extension will allow full regulatory-grade flood-risk assessment in accordance with EVRS-aligned European standards.

Data Availability. All DEM datasets analyzed in this study are openly accessible: SRTM, ALOS AW3D30, Copernicus GLO-30, FABDEM, TanDEM-X, NASADEM, and ASTER GDEM. ICESat-2 ATL03/ATL08 photon and terrain data were obtained from NASA's NSIDC DAAC.

All processed accuracy metrics, stratified statistical results, and DEM-based flood-extent comparisons are publicly available through the interactive platform: GeoHydroAI DEM Dashboard — https://www.geohydroai.org/dem/dashboard.

References

Afrasteh, Y., Slobbe, D.C., Sacher, M., Verlaan, M., Jahanmard, V., Klees, R., Guarneri, H., Keyzer, L., Pietrzak, J., Snellen, M., & Zijl, F. (2023). Realizing the European Vertical Reference System using model-based hydrodynamic leveling data. *Journal of Geodesy, 97*, 86. https://doi.org/10.1007/s00190-023-01778-2.

Airbus Defence and Space GmbH. (2022). Copernicus Digital Elevation Model. Product handbook (Version 5.0, Campaign ID: GEO.2018-1988-2). Retrieved from https://dataspace.copernicus.eu/sites/default/files/media/files/2024-06/geo1988-copernicusdem-spe-002_producthandbook_i5.0.pdf.

Alganci, U., Besol, B., & Sertel, E. (2018). Accuracy assessment of different digital surface models. *ISPRS International Journal of Geo-Information, 7*(3), 114. https://doi.org/10.3390/ijgi7030114.

Arash, A.M., & Yasi, M. (2022). The assessment

for selection and correction of RS-based DEMs and 1D and 2D HEC-RAS models for flood mapping in different river types. *Journal of Flood Risk Management, 16*(1), e12871. https://doi.org/10.1111/jfr3.12871.

Aristizabal, F., Chegini, T., Petrochenkov, G., Salas, F., & Judge, J. (2024). Effects of high-quality elevation data and explanatory variables on the accuracy of flood inundation mapping via Height Above Nearest Drainage. *Hydrology and Earth System Sciences, 28*, 1287—1315. https://doi.org/10.5194/hess-28-1287-2024.

Baugh, C.A., Bates, P.D., Schumann, G.J.-P., & Trigg, M.A. (2013). SRTM vegetation removal and hydrodynamic modeling accuracy. *Water Resources Research, 49*(8), 5276—5289. https://doi.org/10.1002/wrcr.20412.

Carabajal, C.C., & Harding, D.J. (2006). SRTM C-Band and ICESat laser altimetry elevation comparisons as a function of tree cover and relief. *Photogrammetric Engineering & Remote Sensing, 72*(3), 287—298. https://doi.org/10.14358/PERS.72.3.287.

Chen, Y., Wilson, J.P., Zhu, Q., & Zhou, Q. (2012). Comparison of drainage-constrained methods for DEM generalization. *Computers & Geosciences, 48*, 41—49. https://doi.org/10.1016/j.cageo.2012.05.002.

Denker, H. (2015). A new European gravimetric (quasi)geoid EGG2015. *Poster presented at the XXVI General Assembly of the International Union of Geodesy and Geophysics (IUGG), Prague, Czech Republic*. Retrieved from https://www.isgeoid.polimi.it/Geoid/Europe/IUGG_2015_EGG2015.pdf.

Denker, H., Timmen, L., Voigt, C., Weyers, S., Peik, E., Margolis, H.S., Delva, P., Wolf, P., & Petit, G. (2018). Geodetic methods to determine the relativistic redshift at the level of 10^{-18} in the context of international timescales: A review and practical results. *Journal of Geodesy, 92*, 487—516. https://doi.org/10.1007/s00190-017-1075-1.

Duke, G.D., Kienzle, S.W., Johnson, D.L., & Byrne, J.M. (2003). Improving Overland Flow Routing by Incorporating Ancillary Road Data into Digital Elevation Models. *Journal of Spatial Hydrology, 3*(2), article 2.

European Parliament and Council of the European Union. (2007). Directive 2007/60/EC of the European Parliament and of the Council of 23 October 2007 on the assessment and management of flood risks. *Official Journal of the European Union, L288*, 27—34. Retrieved from http://data.europa.eu/eli/dir/2007/60/oj.

European Commission. (2014). INSPIRE data specification on elevation — Technical guidelines. INSPIRE Thematic Working Group Elevation. Retrieved from https://knowledgebase.inspire.ec.europa.eu/publications/inspire-data-specification-elevation-technical-guidelines_en.

Farooq, M., Shafique, M., & Khattak, M.S. (2019). Flood hazard assessment and mapping of River Swat using HEC-RAS 2D model and high-resolution 12-m TanDEM-X DEM (WorldDEM). *Natural Hazards, 97*, 477—492. https://doi.org/10.1007/s11069-019-03638-9.

Garousi-Nejad, I., Tarboton, D.G., Aboutalebi, M., & Torres-Rua, A.F. (2019). Terrain analysis enhancements to the height above nearest drainage flood inundation mapping method. *Water Resources Research, 55*(10), 7983—8009. https://doi.org/10.1029/2019WR024837.

Gdulová, K., Marešová, J., & Moudrý, V. (2020). Accuracy assessment of the global TanDEM-X digital elevation model in a mountain environment. *Remote Sensing of Environment, 241*, 111724. https://doi.org/10.1016/j.rse.2020.111724.

FEMA. (2016). Guidance document 27: Automated engineering — Vertical accuracy requirements (SID 43). Federal Emergency Management Agency. Retrieved from https://www.fema.gov/sites/default/files/2020-02/Elevation_Guidance_May_2016.pdf.

Gesch, D.B. (2018). Best practices for elevation-based assessments of sea-level rise and coastal flooding exposure. *Frontiers in Earth Science, 6*, 230. https://doi.org/10.3389/feart.2018.00230.

GeoHydroAI. (2025). Global DEM accuracy dashboard: Ukrainian Carpathians. [Web application]. GeoHydroAI Platform. Retrieved from https://www.geohydroai.org/dem/dashboard.

Godbout, L., Zheng, J.Y., Dey, S., Eyelade, D., Maidment, D., & Passalacqua, P. (2019). Error assessment for Height Above the Nearest Drainage inundation mapping. *Journal of*

the American Water Resources Association, 55(4), 952—963. https://doi.org/10.1111/1752-1688.12783.

Guenther, E., Magruder, L., Neuenschwander, A., Maze-England, D., & Dietrich, J. (2024). Improving TanDEM-X DTMs with deep learning and ICESat-2 in dense vegetation. *Remote Sensing of Environment, 311*, 114293. https://doi.org/10.1016/j.rse.2024.114293.

Guth, P.L., Van Niekerk, A., Grohmann, C.H., Muller, J.-P., Hawker, L., Florinsky, I.V., Gesch, D., Reuter, H.I., Herrera-Cruz, V., Riazanoff, S., López-Vázquez, C., Carabajal, C.C., Albinet, C. & Strobl, P. (2021). Digital elevation models: Terminology and definitions. *Remote Sensing, 13*(18), 3581. https://doi.org/10.3390/rs1318358.

Han, M., Enwright, N.M., Gesch, D.B., Stoker, J.M., Danielson, J.J., & Amante, C.J. (2024). Assessing the vertical accuracy of digital elevation models by quality level and land cover. *Remote Sensing Letters, 15*(7), 667—677. https://doi.org/10.1080/2150704X.2024.2368924.

Hawker, L., Neal, J., & Bates, P. (2019). Accuracy assessment of the TanDEM-X 90 Digital Elevation Model for selected floodplain sites. *Remote Sensing of Environment, 232*, 111319. https://doi.org/10.1016/j.rse.2019.111319.

Hawker, L., Bates, P., Neal, J., & Rougier, J. (2018). Perspectives on digital elevation model (DEM) simulation for flood modeling in the absence of a high-accuracy open access global DEM. *Frontiers in Earth Science, 6*, 233. https://doi.org/10.3389/feart.2018.00233.

Hawker, L., Uhe, P., Paulo, L., Sosa, J., Savage, J., Sampson, C., & Neal, J. (2022). A 30 m global map of elevation with forests and buildings removed. *Environmental Research Letters, 17*(2), 024016. https://doi.org/10.1088/1748-9326/ac4d4f.

He, L., Pang, Y., Zhang, Z., Liang, X., & Chen, B. (2023). ICESat-2 data classification and estimation of terrain height and canopy height. *International Journal of Applied Earth Observation and Geoinformation, 118*, 103233. https://doi.org/10.1016/j.jag.2023.103233.

Hirt, C., Filmer, M.S., & Featherstone, W.E. (2010). Comparison and validation of the recent freely available ASTER-GDEM ver1, SRTM ver4.1 and GEODATA DEM-9S ver3 digital elevation models over Australia. *Australian Journal of Earth Sciences, 57*(3), 337—347. https://doi.org/10.1080/08120091003677553.

Hu, A., & Demir, I. (2021). Real-time flood mapping on client-side web systems using HAND model. *Hydrology, 8*(2), 65. https://doi.org/10.3390/hydrology8020065.

Höhle, J., & Höhle, M. (2009). Accuracy assessment of digital elevation models by means of robust statistical methods. *ISPRS Journal of Photogrammetry and Remote Sensing, 64*(4), 398—406. https://doi.org/10.1016/j.isprsjprs.2009.02.003.

IGN. (2021). RGE ALTI 1 m [Data set]. Institut national de l'information géographique et forestière. Retrieved from https://geoservices.ign.fr/rgealti.

JAXA. (2021). ALOS global digital surface model (DSM): ALOS World 3D-30 m (AW3D30) Version 3.2/3.1 product description (Edition 1.2). Earth Observation Research Center, Japan Aerospace Exploration Agency.

Kenward, T., Lettenmaier, D.P., Wood, E.F., & Fielding, E. (2000). Effects of digital elevation model accuracy on hydrologic predictions. *Remote Sensing of Environment, 74*(3), 432—444. https://doi.org/10.1016/S0034-4257(00)00136-X.

Kovalchuk, I.P., Lukianchuk, K.A., & Bogdanets, V.A. (2019). Assessment of open source digital elevation models (SRTM-30, ASTER, ALOS) for erosion processes modeling. *Journal of Geology, Geography and Geoecology*, *28*(1), 95—105. https://doi.org/10.15421/111911.

LAWA. (2010). Recommendations for the establishment of flood hazard maps and flood risk maps. German Working Group on Water Issues (LAWA). Retrieved from https://www.lawa.de/documents/lawa_hwgk15062010_text_germany_eng_1552299627.pdf.

Liu, K., Song, C., Ke, L., Jiang, L., Pan, Y., & Ma, R. (2019). Global open-access DEM performances in Earth's most rugged region High Mountain Asia: A multi-level assessment. *Geomorphology, 338*, 16—26. https://doi.org/10.1016/j.geomorph.2019.04.012.

Li, H., Zhao, J., Yan, B., Yue, L., & Wang, L. (2022). Global DEMs vary from one to another: An

evaluation of newly released Copernicus, NASA and AW3D30 DEM on selected terrains of China using ICESat-2 altimetry data. *International Journal of Digital Earth, 15*(10), 1149—1168. https://doi.org/10.1080/17538947.2022.2094002.

Li, Z., Zhu, Q., & Gold, C. (2005). *Digital terrain modeling: Principles and methodology*. CRC Press, 320 p.

Liu, A., Cheng, X., & Chen, Z. (2021). Performance evaluation of GEDI and ICESat-2 laser altimeter data for terrain and canopy height retrievals. *Remote Sensing of Environment, 264*, 112571. https://doi.org/10.1016/j.rse.2021.112571.

Marjańska, D., Olszak, T., & Piętka, D. (2019). Validation of European Gravimetric Geoid models in context of realization of EVRS system in Poland. *Geodesy and Cartography, 68*(2), 329—347. https://doi.org/10.24425/gac.2019.128461.

Markus, T., Neumann, T., Martino, A., Abdalati, W., Brunt, K., Csatho, B., Farrell, S., Fricker, H., Gardner, A., Harding, D., Jasinski, M., Kwok, R., Magruder, L., Lubin, D., Luthcke, S., Morison, J., Nelson, R., Neuenschwander, A., Palm, S., Popescu, S., Shum, CK., Schutz, B.E., Smith, B., Yang, Y., & Zwally, J. (2017). The Ice, Cloud, and land Elevation Satellite-2 (ICESat-2): Science requirements, concept, and implementation. *Remote Sensing of Environment, 190*, 260—273. https://doi.org/10.1016/j.rse.2016.12.029.

Meadows, M., Jones, S., & Reinke, K. (2024). Vertical accuracy assessment of freely available global DEMs (FABDEM, Copernicus DEM, NASADEM, AW3D30 and SRTM) in flood-prone environments. *International Journal of Digital Earth, 17*(1), 2308734. https://doi.org/10.1080/17538947.2024.2308734.

Mesa-Mingorance, J.L., & Ariza-López, F.J. (2020). Accuracy assessment of digital elevation models (DEMs): A critical review of practices of the past three decades. *Remote Sensing, 12*(16), 2630. https://doi.org/10.3390/rs12162630.

Ministry of Internal Affairs of Ukraine. (2018). On the approval of the Methodology for developing flood hazard and flood risk maps (Order No. 153 of 28 February 2018). Retrieved from https://zakon.rada.gov.ua/go/z0350-18.

Moges, D.M., Virro, H., Kmoch, A., Cibin, R., Rohith, A.N., Martínez-Salvador, A., Conesa-García, C., & Uuemaa, E. (2023). How does the choice of DEMs affect catchment hydrological modeling? *Science of the Total Environment, 892*, 164627. https://doi.org/10.1016/j.scitotenv.2023.164627.

Mokhtar, E.S., Pradhan, B., Ghazali, A.H., & Shafri, H.Z.M. (2018). Assessing flood inundation mapping through estimated discharge using GIS and HEC-RAS model. *Arabian Journal of Geosciences, 11*, 682. https://doi.org/10.1007/s12517-018-4040-2.

Munir, B.A., Ahmad, S.R., & Hafeez, S. (2020). Integrated hazard modeling for simulating torrential stream response to flash flood events. *ISPRS International Journal of Geo-Information, 9*(1), 1. https://doi.org/10.3390/ijgi9010001.

Neal, J.C., Bates, P.D., Fewtrell, T.J., Hunter, N.M., Wilson, M.D., & Horritt, M.S. (2009). Distributed whole city water level measurements from the Carlisle 2005 urban flood event and comparison with hydraulic model simulations. *Journal of Hydrology, 368*(1-4), 42—55. https://doi.org/10.1016/j.jhydrol.2009.01.026.

Neal, J., Hawker, L., Uhe, P., Paulo, L., Sosa, J., Savage, J., & Sampson, C. (2023). *FABDEM v1-2*. University of Bristol Research Data Repository. https://doi.org/10.5523/bris.s5hqmjcdj8yo2ibzi9b4ew3sn.

Neuenschwander, A.L., & Pitts, K. (2019). The ATL08 land and vegetation product for the ICESat-2 Mission. *Remote Sensing of Environment, 221*, 247—259. https://doi.org/10.1016/j.rse.2018.11.005.

Neuenschwander, A., Magruder, L., Pitts, K., & Hancock, D. (2020). Validating ICESat-2 terrain and canopy heights in boreal forests using airborne lidar. *Remote Sensing of Environment, 251*, 112110. https://doi.org/10.1016/j.rse.2020.112110.

Nobre, A.D., Cuartas, L.A., Hodnett, M., Rennó, C.D., Rodrigues, G., Silveira, A., & Saleska, S. (2011). Height Above the Nearest Drainage: A hydrologically relevant new terrain model. *Journal of Hydrology, 404*(1-2), 13—29. https://doi.org/10.1016/j.jhydrol.2011.03.051.

Postelniak, A.A. (2013). Accuracy assessment of digital elevation models SRTM and ASTER GDEM. *Journal of Geodesy and Cartography*, (4), 17—21 (in Ukrainian).

Rizzoli, P., Martone, M., Gonzalez, C., Wecklich, C., Borla Tridon, D., Bräutigam, B., Bachmann, M., Schulze, D., Fritz, T., Huber, M., Wessel, B., Krieger, G., Zink, M., & Moreira, A. (2017). Generation and performance assessment of the global TanDEM-X digital elevation model. *ISPRS Journal of Photogrammetry and Remote Sensing, 132*, 119—139. https://doi.org/10.1016/j.isprsjprs.2017.08.008.

Rodriguez, E., Morris, C.S., & Belz, J.E. (2006). A global assessment of the SRTM performance. *Photogrammetric Engineering & Remote Sensing*, 72(3), 249—260. https://doi.org/10.14358/PERS.72.3.249.

Sampson, C.C., Smith, A.M., Bates, P.D., Neal, J.C., & Trigg, M.A. (2016). Perspectives on open access high resolution digital elevation models to produce global flood hazard layers. *Frontiers in Earth Science*, 3, 85. https://doi.org/10.3389/feart.2015.00085.

Smith, B., Adusumilli, S., Csathó, B.M., Felikson, D., Fricker, H.A., Gardner, A., Holschuh, N., Lee, J., Paolo, F.S., Siegfried, M.R., Sutterley, T., & the ICESat-2 Science Team. (2023). ATLAS/ICESat-2 L3A land ice height, Version 6. NASA National Snow and Ice Data Center Distributed Active Archive Center. https://doi.org/10.5067/ATLAS/ATL06.006.

Stoleriu, C.C., Urzica, A., & Mihu-Pintilie, A. (2020). Improving flood risk map accuracy using high-density LiDAR data and the HEC-RAS river analysis system: A case study from north-eastern Romania. *Journal of Flood Risk Management, 13*(S1), e12572. https://doi.org/10.1111/jfr3.12572.

Swinski, J.P., Lidwa, E., Sutterley, T., Ugarte, C.E., Henderson, S., Shean, D., Gearon, J.J., Shiklomanov, A., Corcoran, F., Kennedy, J.H., Sharonin, K., & Hugonnet, R. (2025). *Slide Rule Earth/slide rule: v4.13.3* (Version 4.13.3). Retrieved from https://client.sliderule earth.io/landing.

Uuemaa, E., Ahi, S., Montibeller, B., Muru, M., & Kmoch, A. (2020). Vertical accuracy of freely available global digital elevation models (ASTER, AW3D30, MERIT, TanDEM-X, SRTM, and NASADEM). *Remote Sensing, 12*(21), 3482. https://doi.org/10.3390/rs12213482.

Wechsler, S.P. (2003). Perceptions of digital elevation model uncertainty by DEM users. *URISA Journal, 15*(2), 57—64.

Wilson, J.P., & Gallant, J.C. (Eds.). (2000). *Terrain analysis: Principles and applications*. Wiley, 524 p.

Xu, K., Fang, J., Fang, Y., Sun, Q., Wu, C., & Liu, M. (2021). The importance of digital elevation model selection in flood simulation and a proposed method to reduce DEM errors: A case study in Shanghai. *International Journal of Disaster Risk Science, 12*, 890—902. https://doi.org/10.1007/s13753-021-00377-z.

Zablotskyi, F., Dzhuman, B., & Brusak, I. (2021). On the accuracy of geoid (quasigeoid) models relative to the UELN/EVRS2000 height system. *Modern advances in geodetic science and production, 1*(41), 28—34 (in Ukrainian).

Zhu, H., & Chen, Y. (2024). A Study of the Effect of DEM Spatial Resolution on Flood Simulation in Distributed Hydrological Modeling. *Remote Sensing, 16*(16), 3105. https://doi.org/10.3390/rs16163105.

Zhou,Q. (2017). Digital elevation model and digital surface model. In D. Richardson et al. (Eds.), *The international encyclopedia of geography*. John Wiley & Sons. https://doi.org/10.1002/9781118786352.wbieg0768.

Zhou, Q., & Li, J. (2020). Geo-Spatial Analysis in Hydrology. *ISPRS International Journal of Geo-Information, 9*(7), 435. https://doi.org/10.3390/ijgi9070435.

Zhou, Q., Zhang, F., & Cheng, L. (2018). A data-driven method for the determination of water-flow velocity in watershed modelling. *PeerJ Preprints, 6*, e27155v1. https://doi.org/10.7287/peerj.preprints.27155v1.

Валідація глобальних цифрових моделей рельєфу за даними ICESat-2 LiDAR у задачах моделювання заплав в Українських Карпатах

В.В. Нікоряк, В.В. Осипов, Н.М. Осадча, 2026

Український гідрометеорологічний інститут, Київ, Україна

Точні топографічні дані є основою гідрологічного моделювання затоплення заплав у гірських умовах, де круті схили та густий лісовий покрив підсилюють вертикальні похибки глобальних цифрових моделей рельєфу (DEM). Виконано комплексну валідацію відкритих DEM — SRTM v3, NASADEM, ASTER GDEM v2, ALOS AW3D30, Copernicus GLO-30, FABDEM та TanDEM-X — за допомогою високоточної лідарної альтиметрії супутника Ice, Cloud, and Land Elevation Satellite-2 (ICESat-2) у межах Українських Карпат. Для забезпечення геодезичної узгодженості всі DEM та спостереження ICESat-2 були попередньо приведені до Європейської вертикальної референтної системи (EVRS) шляхом використання високоточної європейської гравіметричної квазігеоїдної моделі EGG2015.

Залишки висот було кількісно оцінено із застосуванням як класичних (середня похибка, середньоквадратична похибка), так і робастних (нормалізоване медіанне абсолютне відхилення) статистичних метрик у поєднанні з аналізом, стратифікованим за рельєфними умовами на основі крутості схилів, типів земного покриву та гідрологічного положення, визначеного за моделлю висоти над найближчим дренажем (HAND). Результати показують, що похибки DEM значною мірою визначаються крутістю рельєфу та рослинним покривом, причому зі зростанням крутизни спостерігається нелінійне зростання похибок.

Серед досліджених наборів даних FABDEM продемонструвала найменшу середню похибку (≈1,5 м) і найвищу стабільність у всіх класах схилів. Натомість SRTM і NASADEM систематично завищують висоти в лісових районах унаслідок впливу рослинного покриву. Copernicus GLO-30 та ALOS AW3D30 характеризуються помірною точністю, однак їхня якість суттєво погіршується на схилах понад 15°. ASTER GDEM показала найбільшу варіабельність та екстремальні похибки, особливо в умовах складного рельєфу.

Гідрологічний аналіз засвідчив, що невизначеності, пов'язані з DEM, безпосередньо впливають на результати моделювання заплав. У критичній зоні HAND 0—6 м вертикальні похибки (5—10 м) зіставні або перевищують типові глибини затоплення, що призводить до суттєвих розбіжностей у визначенні площ затоплення, геометрії русла та гідравлічних параметрів.

Дослідження також показало, що відповідність міжнародним стандартам точності (INSPIRE, FEMA, LAWA) зазвичай досягається лише для рівнинних територій, тоді як більшість глобальних DEM не відповідають вимогам у гірських регіонах. Це підкреслює необхідність використання моделей типу DTM або лідарних даних для нормативного картування ризику затоплень.

Для забезпечення відтворюваності та масштабованості аналізу запропоновано фреймворк GeoHydroAI — інтегроване геопросторове аналітичне середовище, що поєднує обробку даних ICESat-2 через SlideRule, аналіз різниць DEM із використанням xDEM, морфометричний аналіз за допомогою WhiteboxTools та високопродуктивні просторові запити на базі DuckDB.

Такий підхід забезпечує автоматизовану валідацію, аналіз похибок із урахуванням умов рельєфу та інтерактивне дослідження невизначеностей DEM у межах геоморфологічних і гідрологічних градієнтів. Запропонований фреймворк формує

відтворюваний стандарт оцінювання DEM і створює базовану на даних основу для оцінювання ризику затоплень і гідрологічного моделювання в гірських регіонах із обмеженими даними. Крім того, інтеграція геодезичного забезпечення (EVRS/EGG2015), супутникової альтиметрії (ICESat-2) і геоморфологічного аналізу формує фізично узгоджену основу представлення рельєфу в гідрологічних застосуваннях. Це дослідження розглядає валідацію DEM як ключовий компонент GeoAI-орієнтованого екологічного моделювання, поєднуючи геодезію, дистанційне зондування Землі та гідравлічне моделювання в єдиній аналітичній парадигмі.

Ключові слова: цифрова модель рельєфу (DEM), SRTM, Copernicus GLO-30, NASADEM, ALOS AW3D30, FABDEM, HAND, моделювання заплав, гідрологічна точність, GeoHydroAI, Українські Карпати.